2011-12-31

Imaging transport in nanowires using near-field detection of light

Haegel, N.M.

Elsevier B.V.

Journal of Crystal Growth 352 (2012), p. 218-223
http://hdl.handle.net/10945/48346

Journal of Crystal Growth 352 (2012) 218–223

Contents lists available at SciVerse ScienceDirect

Journal of Crystal Growth

journal homepage: www.elsevier.com/locate/jcrysgro

Imaging transport in nanowires using near-field detection of light

N.M. Haegel *, D.J. Chisholm, R.A. Cole

Department of Physics, Naval Postgraduate School, 833 Dyer Road, Monterey, CA 93943, USA

ARTICLE INFO

Available online 31 December 2011

Keywords:
A1. Characterization
A1. Diffusion
A1. Nanostructures
A1. Optical microscopy
B2. Semiconducting II–VI materials

ABSTRACT

Major progress in the crystal growth of nanowires and related structures places new demands on our abilities to characterize optical and electronic properties with both an ease and a resolution commensurate with the materials of interest. In particular, transport properties, such as minority carrier diffusion length, are important for a range of applications in light emission, sensing and solar energy conversion. In this paper, a technique to "image transport" in nanostructures by monitoring the motion of charge via the recombination emission of light is reviewed. Transport imaging combines the resolution of near-field optics with the charge generation control of a scanning electron microscope. The technique is related to, but significantly different from standard cathodoluminescence, since it maintains the spatial information of the emitted light. Light is collected in the near-field from a scanning fiber in an atomic force microscope/near-field scanning optical microscope system. It is possible to determine minority carrier or exciton diffusion lengths from a single optical image, without any electrical contact to the sample. New results are presented for minority carrier hole transport in ZnO nanowires and nanobelts.

Published by Elsevier B.V.

1. Introduction

The tremendous progress in the growth and synthesis of nanoscale materials has simultaneously posed new challenges and placed new demands on characterization capabilities. For nanowires, nanorods, nanobelts or nanoribbons of interest for both light emitting devices, such as LEDs and lasers, and light collection devices, such as solar cells and photodetectors, the transport of minority carriers plays an important role in device performance. Conventional means of measuring minority carrier diffusion lengths, such as electron beam induced current (EBIC) techniques, or full scale device characterization, generally require contacts and associated processing. Crystal growers would benefit from techniques that could provide electronic transport information with a spatial scale commensurate with the materials of interest, but without requiring additional electrical contacting, which is often challenging and time-consuming for individual nanostructures.

We describe in this paper an approach to measurement of minority carrier transport in nanowires, using a technique called transport imaging. Transport imaging combines scanning electron microscopy (SEM) and optical microscopy to "see" electronic transport via imaging of non-equilibrium carrier recombination. Spatially resolved imaging of resulting luminescence allows observation of the motion of that charge, acquiring steady-state images of the light emitted as some fraction of carriers recombine along their path of travel. While some related experiments have utilized a laser source for generation of charge [1–3], we have more recently utilized this approach at very high spatial resolution for the study of transport in nanostructures by integrating near-field optical microscopy, which provides spatial resolution beyond the far-field diffraction limit, with the high resolution and spatial control of an electron beam in an SEM for generation of charge [4,5].

The approach is related to, but distinct from, cathodoluminescence in that it maintains the spatial information of the recombination light, which is generally lost in traditional scanning photoluminescence or cathodoluminescence. In these techniques, spatial resolution comes from moving the source of excitation. In transport imaging, the source of excitation is fixed and spatial information comes from the distribution of the associated recombination. In essence, it is an optical form of the famous Haynes–Shockley experiment [6], but one with very high spatial resolution that can often be performed without any electrical contact to the sample. Early work applied this approach to the study of transport and field dependent mobilities and anisotropies in ordered materials [7–10].

Transport imaging in an SEM allows for direct measure of the mobility–lifetime ($\mu\tau$) product of the non-equilibrium carriers created by the incident electron beam. In the absence of an electric field (i.e., when the technique is applied in a contact-free manner), minority carriers (or excitons depending

* Corresponding author. Tel.: +1 831 656 3954; fax: +1 831 656 2834.
E-mail address: nmhaegel@nps.edu (N.M. Haegel).

0022-0248/$ - see front matter Published by Elsevier B.V.
doi:10.1016/j.jcrysgro.2011.12.067

on temperature and exciton binding energy) will diffuse from their point of origin. The subsequent luminescence distribution reflects the diffusion length, whatever the dominant mechanism that controls the minority carrier or exciton lifetime. In the presence of an electric field, both carrier drift and diffusion come into play.

The basic idea is illustrated in Fig. 1, which shows minority carrier (hole) diffusion and drift in a high purity sample of thick ($\sim$80 μm) liquid phase epitaxial material on a semi-insulating GaAs substrate [7]. The carrier generation point, in all cases, is a single spot, using a 20 keV electron beam. The composite figure shows the effect of diffusion only (top image) and then combined drift and diffusion in an alternating electric field ($\pm$80 V/mm). The quasi-bulk nature of the transport in this relatively thick film makes extraction of diffusion length a numerical analysis problem requiring a multi-parameter least squares fitting approach to a three-dimensional half-space problem [11]. In nanowires, however, the analysis for transport in restricted dimensions is relatively straight-forward and transport imaging offers a direct measure of minority carrier transport properties that can provide early stage feedback for crystal growers. Section 2 will describe the experimental approach and a new system for near-field transport imaging and then Section 3 will present results for diffusion in ZnO nanowires and nanobelts.

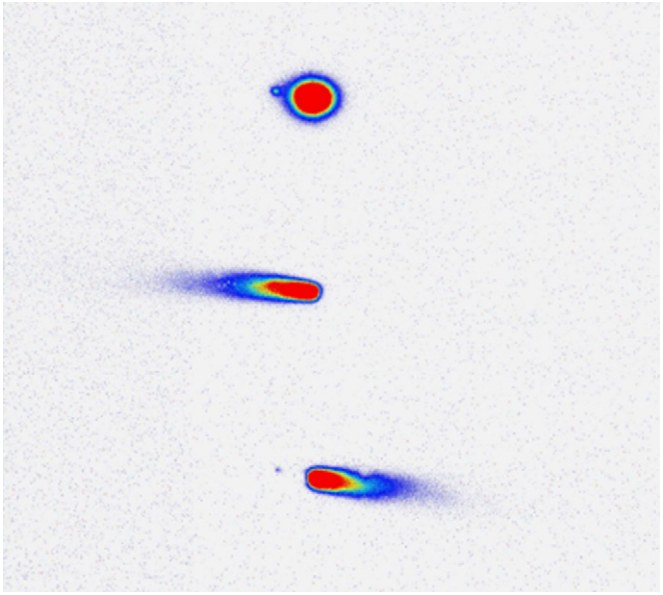

Fig. 1. Spatially resolved luminescence images showing effect of diffusion (upper) and combined diffusion and drift (center and lower) of minority carrier holes in an n-type GaAs epitaxial layer. Electron beam energy is 20 keV. Image width is 400 μm and the bias for the drift images is $\pm$80 V/mm.

2. Experimental approach—NSOM and SEM integration

An integrated transport imaging facility has recently been developed at the Naval Postgraduate School that combines an FEI field emission microscope (Inspect 50) with a Nanonics Multiview 2000 atomic force/near-field optical scanning (AFM/NSOM) microscope. The Multiview 2000 architecture enables integration with the SEM to provide direct optical axis access to the sample for electron beam imaging as well as charge carrier generation. Cantilevered fiber probes are used simultaneously as AFM topography probes and near-field collection tips, with apertures ranging from 100 to 500 nm. Aperture size at the tip of the fiber determines the resolution for the transport images and the smallest size is desirable for maximum resolution. In practice, this is limited by the intensity of the luminescence and the strong dependence of collection efficiency on aperture diameter.

Fig. 2 shows a schematic diagram (A) of the apparatus and a SEM image (B) of an NSOM probe above a sample with a mixture of ZnO nanowires and nanobelts. The light collected via the NSOM tip exits through a vacuum fiber feedthrough and is detected by an external Si photodiode or photomultiplier tube, depending on the desired wavelength detection range. Positioning of the tip with respect to the nanostructure of interest is accomplished via the "inertial motion" feature of the Multiview 2000, which allows for motion of the sample relative to the probe tip via pulsed motion of the sample for a maximum travel of $\sim$6 mm. Using this capability, all the individual structures seen in Fig. 2B could be measured without the need to externally reposition the sample or the NSOM tip.

The SEM serves two distinct purposes. First, it provides a high resolution image of the sample, allowing selection of the nanostructures and imaging of their topographic features. During the actual acquisition of transport imaging data, the SEM is operated in spot or line mode, for localized generation of free carriers. It is critical that the beam location remains fixed, relative to the sample, so we utilize a minimum spot size (probe current) to minimize charging, while at the same time providing sufficient carrier generation for a measureable luminescent signal. The surface of the sample is also grounded via a flexible wire to the SEM ground. With the beam fixed on the sample, the NSOM probe is scanned across the material and a map of the luminescence emission is created. The Multiview 2000 allows for a maximum scanning range of $\sim 100 \times 100\ \mu m^2$. Typical scans, depending on diffusion length and nanostructure size, are $\sim$2–20 μm on a side.

The NSOM probes have the cantilevered fiber glued to a tuning fork. Special attention has been paid to minimizing charging of the glue and to extending the NSOM tips to minimize electron beam distortion effects associated with proximity of the tuning fork. Unlike far-field collection of the luminescence with a microscope and CCD camera, where the full luminescence distribution can be collected, care must be taken in the near-field system to avoid direct excitation of the SiO_2 probe, which will

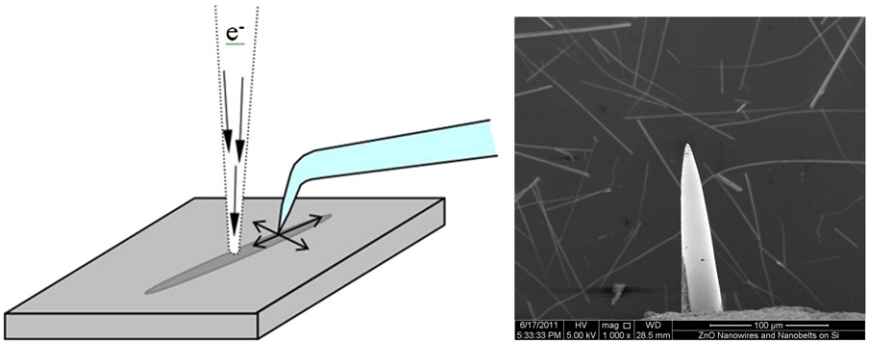

Fig. 2. Schematic diagram showing incident electron beam, NSOM tip and nanowire under study (left) and SEM image of NSOM tip in proximity of ZnO nanostructures.

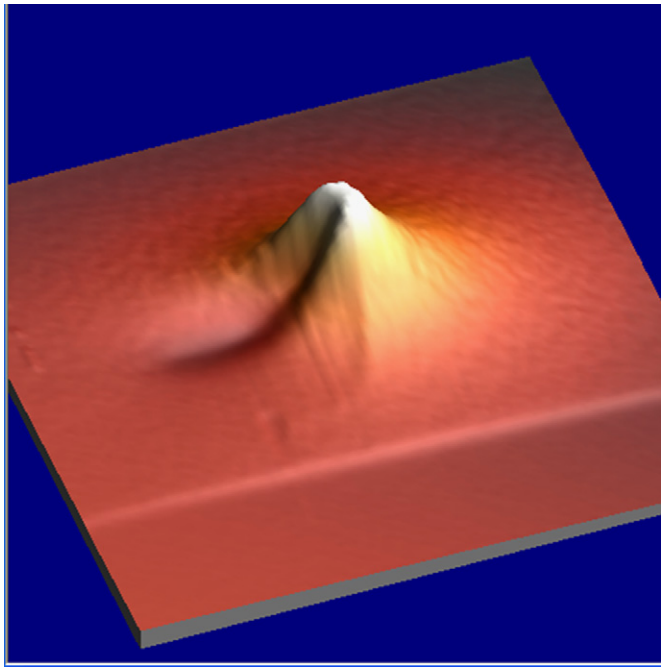

Fig. 3. NSOM image of luminescence distribution from a GaAs double heterostructures under spot mode laser excitation, with intensity (arbitrary units) as the z-axis. Image dimensions are 15×15 μm^2.

produce direct luminescence in the fiber itself. In addition, the collecting probe will block the excitation of the sample over part of the scan.

This effect is shown in Fig. 3, which illustrates NSOM collection of luminescence in a thin film GaAs double heterostructure, excited in this case with above bandgap laser illumination. Although the laser light itself can be eliminated with a filter, the NSOM image shows the asymmetry in collection introduced by the nature of the tip scanning. In a one-dimensional nanowire, the luminescence distribution is simply collected in one direction, beginning adjacent to the point of excitation. Since the luminescence, both at the point of excitation and at subsequent positions along the wire, is emitted in all directions, the light collected by the fiber represents the relatively small fraction that is emitted in the upward direction and within the cone determined by the index of refraction of the material. The remainder will be waveguided along the wire axis. Detection of the waveguided light is often possible at the end of the structure.

3. Transport imaging in ZnO nanowires and nanobelts

To illustrate the approach, we present results on ZnO nanostructures. ZnO is a direct bandgap material, with a room temperature bandgap of 3.37 eV [12,13]. This results in strong luminescence with the band-edge emission around 368 nm and makes ZnO an excellent candidate material for transport imaging.

The nanowires were grown using either hydrothermal growth from solution or physical vapor deposition (PVD). In PVD-growth, the source materials are sublimated in powder form and then deposited on a substrate in a horizontal tube furnace. Hydrothermal growth utilizes crystallization from solution under high pressures. Growth techniques are described in [14] and the extensive references within.

A typical room temperature cathodoluminescence spectrum from the PVD-growth structures is shown in Fig. 4. The defect-related luminescence varies in relative intensity for various

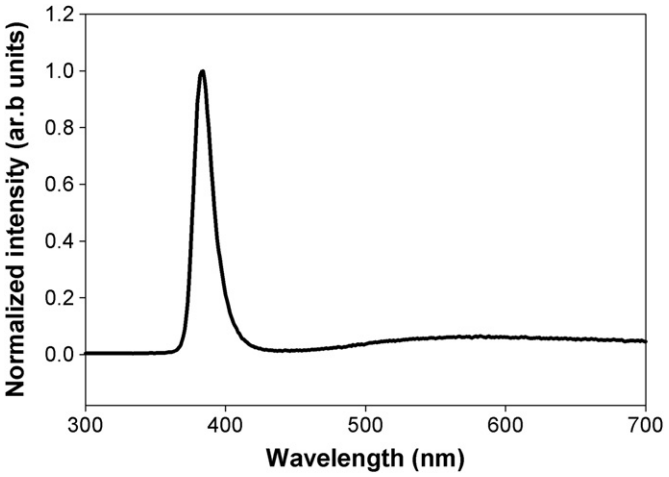

Fig. 4. Cathodoluminescence spectrum (intensity as a function of wavelength) for a PVD-grown ZnO nanowire.

samples, but the band-edge luminescence is generally dominant. For transport imaging, the light is detected with a Perkin Elmer MP-983 photomultiplier detector with a response range from 185 to 650 nm. A UV-optimized fiber is used in the NSOM probe to maximize ultraviolet transmission.

Fig. 5 shows an example of the NSOM image for carrier diffusion in a ZnO PVD wire with a relatively large ($\sim$1 μm) cross-sectional dimension. The electron beam is incident at a spot at the lower left on the wire, not shown in the figure. The incident electron beam energy is 30 keV. Although the electron beam spot size on the surface of the wire is approximately 50 nm, the generation volume produced results in carrier generation over a volume of $\sim$1.0 μm. The NSOM image shows both the luminescence from recombination in the vicinity of the carrier generation point and the waveguided emission emerging from the end, reflecting the shape of the nanowire. One also sees the effect of surface recombination in the spatial variation of the intensity across the wire and the decreased intensity near the surface.

Intensity information is extracted from the NSOM image, with data collected on both the trace and retrace of the scan. In Fig. 6, Intensity is plotted as a function of position, with intensity on a logarithmic scale. For diffusion in one dimension, the intensity adjacent to the generation volume should decrease as

$$I(x) = I_o \exp(-x/L_d)$$

where I is the intensity, x is the position along the wire and L_d represents the effective diffusion length of minority carriers and/or excitons. The effective diffusion length extracted from the data in Fig. 6 is 1050 nm. Similar measurements have been performed on hydrothermally grown ZnO wires (Fig. 7a), which are several microns in length and range from $\sim$400 to 800 nm in diameter, and several PVD-grown nanobelts (Fig. 7b), which are relatively thin (100–300 nm), two dimensional plate-like structures.

Fig. 8 shows the NSOM image for recombination and waveguided emission in a nanobelt, presented in three dimensions, with intensity as the z-axis. The SEM excitation is incident at a spot just above the image, but located in the center of the nanobelt. The background local fluctuations throughout the image are noise in the NSOM signal. Waveguided emission is seen along the edges of the structure. In the nanobelt, diffusion is possible in two dimensions and the diffusion profile is given by

$$I \sim K_o(r/L_d),$$

where K_o is the zeroth order modified Bessel function of the second kind. The Bessel function fit to the luminescence profile along a diameter through the excitation point is shown in Fig. 9.

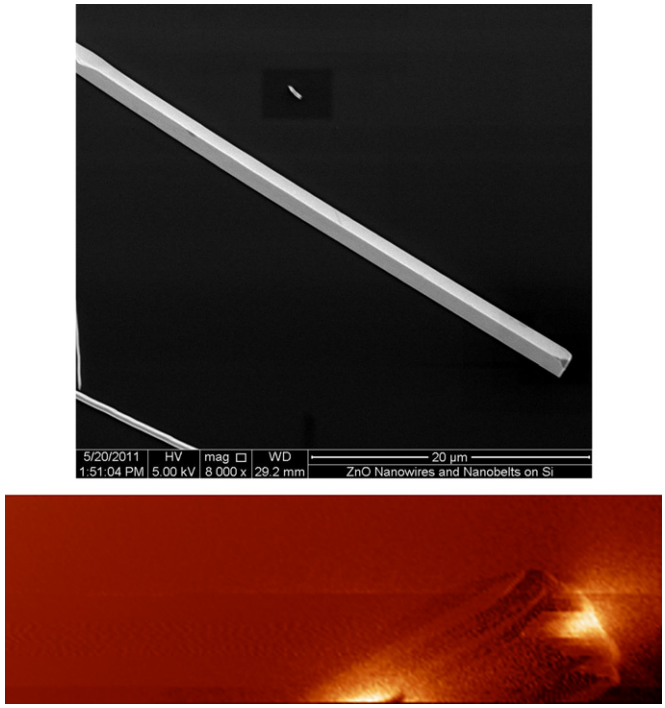

Fig. 5. SEM image (upper) and NSOM transport image (lower) of a PVD-grown ZnO nanowire. The excitation point is fixed at the center of the wire, at a point just below the edge of the NSOM image. Electron beam excitation energy is 30 keV.

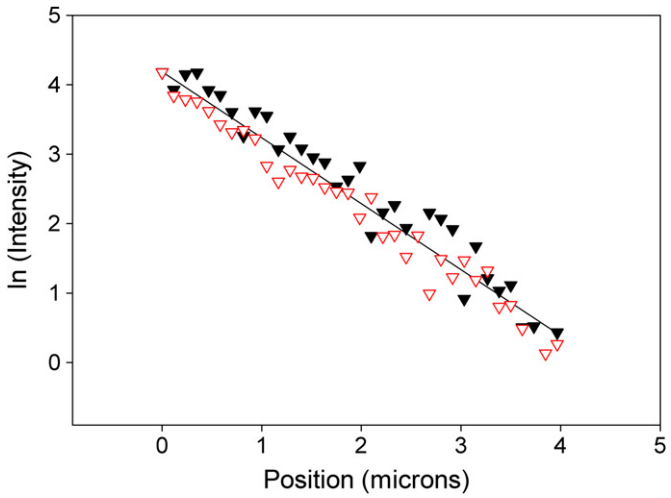

Fig. 6. Natural logarithm of the intensity as a function of position, including intensity measured on both the trace and retrace of the NSOM scan, and the "best fit" linear regression for determination of diffusion length.

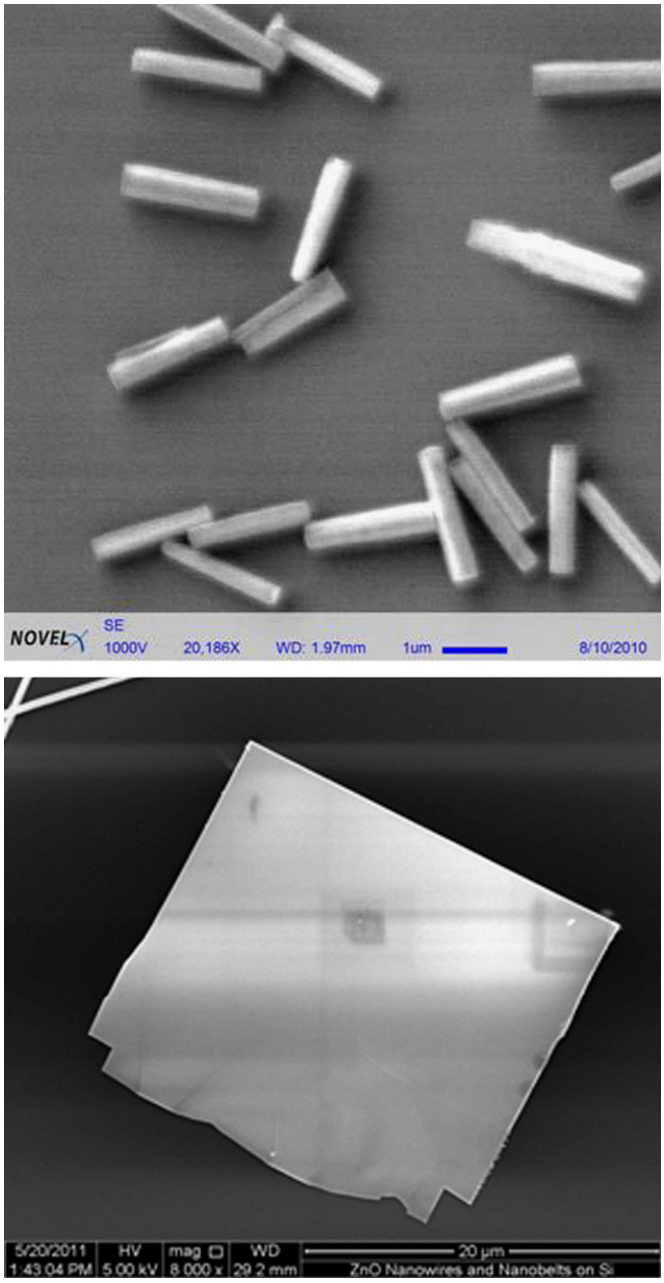

Fig. 7. SEM images of hydrothermally grown ZnO nanowires (upper) and PVD-grown ZnO nanobelts (lower). The scale bars are 1 µm for the upper image and 20 µm for the lower image.

Minority carrier diffusion lengths measured for these various samples are summarized in Table 1. The binding energy of excitons in ZnO is 60 meV [15], and excitons have been shown to be stable in ZnO at room temperature. The diffusion length, therefore, represents the combined motion of minority carriers, whether as free carriers or as excitons, occurring in the wire. Surface recombination will also play a role. Models for the effect of surface recombination on effective lifetime in nanowires are still in development, with some evidence that band bending at the surface [16] may play an important role in some materials. The transport imaging data, therefore, should be interpreted as effective overall diffusion lengths that show the combined effect of bulk and surface recombination effects, in the same way that the effective lifetime in any semiconductor is a combination of the various contributions from radiative and non-radiative recombination arising from multiple sources.

Although we expect variations with diameter and particulars of the crystal growth, the diffusion lengths in the PVD-grown material are consistently longer than in comparison with the diameter of the hydrothermally grown structures. Effective diffusion length also depends on nanowire diameter, consistent with the TRPL studies in GaN [17] and near-field scanning photocurrent measurements in very small diameter ZnO nanowires [18].

We note that the diffusion lengths reported for the nanobelts are as long or longer than the best reported lengths from electron beam induced current (EBIC) measurements for bulk n-type ZnO, which range from 0.4 to 2.4 µm [19,20]. Time resolved photoluminescence measurements on bulk ZnO show multiple exponential behavior, which has been interpreted as potentially

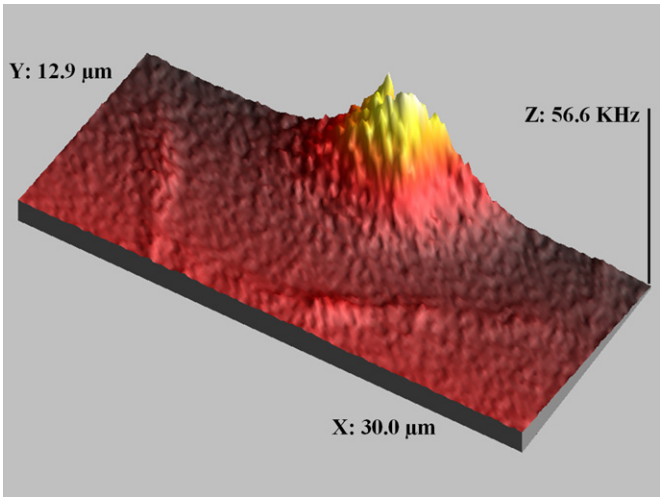

Fig. 8. NSOM transport image showing carrier diffusion and photon waveguiding in a ZnO nanobelt. The excitation point is fixed at a point in the center of the nanobelt, at a position just above the edge of the NSOM image.

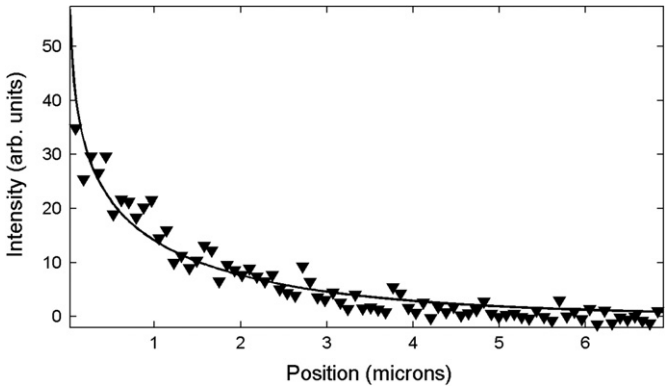

Fig. 9. Intensity distribution along a diameter extending out from the point of carrier generation and the least squares regression fit to a zeroth order modified Bessel function of the second kind.

Table 1
Diffusion lengths measured via transport imaging.

Nanostructure (diameter)	Diffusion length (nm)
Hydrothermal nanowire (600 nm)	150
PVD nanowire (800 nm)	640
PVD nanowire (2000 nm)	1050
Nanobelt (250–350 nm thick)	2080

indicating both free carrier and excitonic recombination. Koida et al. [21] reported that times ranging from 1 to 14 ns, which when combined with the maximum reported mobility to date of $\sim$50 cm^2/V s for holes in ZnO [12], would result in diffusion lengths of 0.36–1.4 μm. Mobility measurements on holes in ZnO, however, have been limited by the challenges associated with p-type doping in this material. Recent EBIC measurements [22] on the collective response of a layer of nanowires in Sb-doped material indicated a room temperature value of $\sim$2.7 μm for L_d, but it would be for minority carrier electrons if a high level of p-type doping has been achieved and therefore is not a direct comparison.

It has been demonstrated, via polarized Raman spectroscopy and TEM, that defect densities in ZnO nanobelts can be very low [23], with regard to both line and point defects, and the diffusion lengths in the ZnO nanobelts measured to date may reflect these low defect densities. Further studies, as a result of nanobelt thickness and growth conditions, will be required.

4. Conclusion

In summary, we present an approach to imaging carrier transport in nanowires using near-field detection of the distribution of the recombination luminescence. The technique provides a contact-free method for investigating minority carrier and/or excitonic transport. This transport imaging capability is enabled by the combination of a near-field scanning optical microscope in a field emission SEM. Results for ZnO nanostructures grown by physical vapor deposition and hydrothermal growth from solution indicate carrier diffusion lengths ranging from 0.15 to 2.8 μm, depending on growth technique and material geometry. Transport imaging should be useful to provide direct feedback to crystal growers on the key transport parameters of interest in a variety of materials with luminescent signatures, without requiring additional device processing.

Acknowledgments

This work was supported at NPS by the National Science Foundation Grant DMR 0804527 and by a grant from the Nano-MEMS program of DARPA (D. Polla, Program Manager). The ZnO nanostructures were synthesized and provided by Dr. Yaguang Wei and Prof. Z.L. Wang, School of Materials Science and Engineering, Georgia Institute of Technology.

References

[1] R.A. Höpfel, J. Shah, P.A. Wolff, A.C. Gossard, Negative absolute mobility of minority electrons in GaAs quantum-wells, Physical Review Letters 56 (1986) 2736–2739.
[2] F.P. Logue, D.T. Fewer, S.J. Hewlett, C. Jordan, J.F. Donegan, E.M. McCabe, J. Hegarty, S. Taniguchi, T. Hino, K. Nakano, A. Ishibashi, Optical measurement of the ambipolar diffusion length in a ZnCdSe–ZnSe quantum well, Journal of Applied Physics 81 (1997) 536–538.
[3] Thomas D. Boone, Hironori Tsukamoto, Jerry M. Woodall, Intensity and spatial modulation of spontaneous emission in GaAs by field aperture selecting transport, Applied Physics Letters 82 (2003) 3197–3199.
[4] Nancy M. Haegel, Chun-Hong Low, Lee Baird, Goon-Hwee Ang, Transport imaging with near field optical scanning microscopy, in: SPIE Proceedings, vol. 7378: Scanning Microscopy, 2009.
[5] C.P. Lee Baird, R. Ong, N.M. Adam Cole, A.Alec Haegel, Qiming Talin, Li, George T. Wang, Transport imaging for contact-free measurements of minority carrier diffusion in GaN, GaN/AlGaN and GaN/InGaN core–shell nanowires, Applied Physics Letters 98 (2011) 132104.
[6] J.R. Haynes, W. Shockley, The mobility and life of electrons and holes in germanium, Physical Review 81 (1951) 835.
[7] N.M. Haegel, J.D. Fabbri, M.P. Coleman, Direct transport imaging in planar structures, Applied Physics Letters 84 (2004) 1329–1331.
[8] D.R. Luber, F.M. Bradley, N.M. Haegel, M.C. Talmadge, M.P. Coleman, T.D. Boone, Imaging transport for the determination of minority carrier diffusion length, Applied Physics Letters 88 (2006) 163509.
[9] N.M. Haegel, T.J. Mills, M. Talmadge, C. Scandrett, C.L. Frenzen, H. Yoon, C.M. Fetzer, R.R. King, Direct imaging of anisotropic minority-carrier diffusion in GaInP, Journal of Applied Physics 105 (2009) 023711.
[10] N.M. Haegel, S.E. Williams, C.L. Frenzen, C. Scandrett, Minority carrier lifetime variations associated with misfit dislocation networks in heteroepitaxial GaInP, Semiconductor Science and Technology 25 (2010) 055017.
[11] Kevin Blaine, Contact Free Measurement of Mobility–Lifetime ($\mu\tau$) Product using Transport Imaging, M.S. Thesis, Applied Mathematics Department and Physics Department, Naval Postgraduate School, June 2011.
[12] Janotti Anderson, Chris G Van de Walle, Fundamentals of zinc oxide as a semiconductor, Reports on Progress in Physics 72 (2009) 126501.
[13] A. Mang, K. Reimann, St. Ruebenacke, Band gaps, crystal-field splitting, spin-orbit coupling, and exciton binding energies in ZnO under hydrostatic pressure, Solid State Communications 94 (1995) 251.
[14] Zhong Lin Wang, ZnO nanowire and nanobelt platform for nanotechnology, Materials Science and Engineering Reports 64 (2009) 33–71. and references within.
[15] D.C. Reynolds, D.C. Look, B. Jogai, Optically pumped ultraviolet lasing from ZnO, Solid State Communications 99 (1996) 873.

[16] N.A. Sanford, P.T. Blanchard, K.A. Bertness, A. Mansfield, J.B. Schlager, A.W. Sanders, A. Roshko, B.B. Burton, S.M. George, Steady-state and transient photoconductivity in *c*-axis GaN nanowires grown by nitrogen-plasma-assisted molecular beam epitaxy, Journal of Applied Physics 107 (2010) 034310.
[17] John B. Schlager, Kris.A. Bertness, Paul T. Blanchard, Lawrence H. Robins, Alexana Roshko, Norman Sanford, Steady-state and time-resolved photoluminescence from relaxed and strained GaN nanowires grown by catalyst-free molecular-beam epitaxy, Journal of Applied Physics 103 (2008) 124309.
[18] A. Soudi, P. Dhakal, Y. Gu, Diameter dependence of the minority carrier diffusion length in individual ZnO nanowires, Applied Physics Letters 96 (2010) 253115.
[19] O. Lopatiuk, L. Chernyak, A. Isinsky, J.Q. Xie, P.P. Chow, Electron-beam-induced current and cathodoluminescence studies of thermally activated increase for carrier diffusion length and lifetime in n-type ZnO, Applied Physics Letters 87 (2005) 162103.
[20] Olena Lopatiuk-Tirpak, Leonid Chernyak, Studies of minority carrier transport in ZnO, Superlattices and Microstructures 42 (2007) 201.
[21] T. Koida, S.F. Chichibu, A. Uedono, A. Tsukazaki, M. Kawasaki, T. Sota, Y. Segawa, H. Koinuma, Correlation between the photoluminescence lifetime and defect density in bulk and epitaxial ZnO, Applied Physics Letters 82 (2003) 532.
[22] Y. Lin, M. Shatkhin, E. Flitsiyan, L. Chernyak, Z. Dashevsky, S. Chu, J.L. Liu, Minority carrier transport in p-ZnO nanowires, Journal of Applied Physics 109 (2011) 106107.
[23] Marcel Lucas, Zhong Lin Wang, Elisa Riedo, Growth direction and morphology of ZnO nanobelts revealed by combining in situ atomic force microscopy and polarized Raman spectroscopy, Physical Review B 81 (2010) 045415.